AGU PUBLICATIONS

JGR

Journal of Geophysical Research: Solid Earth

RESEARCH ARTICLE

10.1002/2013JB010625

Key Points:
- First implementation of Dynamic Acoustoelastic Testing (DAET) in situ
- Nonlinear elastic parameters of soil can be measured in situ
- DAET is promising for in situ measurement of the nonlinear site response

Correspondence to:
G. Renaud,
renaud_gu@yahoo.fr

Citation:
Renaud, G., J. Rivière, C. Larmat, J. T. Rutledge, R. C. Lee, R. A. Guyer, K. Stokoe, and P. A. Johnson (2014), In situ characterization of shallow elastic nonlinear parameters with Dynamic Acoustoelastic Testing, *J. Geophys. Res. Solid Earth*, *119*, doi:10.1002/2013JB010625.

Received 23 AUG 2013
Accepted 17 AUG 2014
Accepted article online 22 AUG 2014

In situ characterization of shallow elastic nonlinear parameters with Dynamic Acoustoelastic Testing

G. Renaud[1,2], J. Rivière[3], C. Larmat[3], J.T. Rutledge[4], R.C. Lee[3], R.A. Guyer[3,5], K. Stokoe[6], and P.A. Johnson[3]

[1]Department of Biomedical Engineering, Erasmus Medical Center, Rotterdam, Netherlands, [2]Laboratoire d'Imagerie Biomédicale, Sorbonne Universités, UPMC, University Paris 06, Paris, France, [3]Earth and Environmental Sciences, Los Alamos National Laboratory, Los Alamos, New Mexico, USA, [4]Schlumberger, Houston, Texas, USA, [5]Department of Physics, University of Nevada, Reno, Nevada, USA, [6]Department of Civil Engineering, University of Texas at Austin, Austin, Texas, USA

Abstract In situ measurement of the elastic nonlinear site response is advantageous to provide optimal information for prediction of strong ground motion at a site. We report the first implementation of a technique known as Dynamic Acoustoelastic Testing (DAET) in situ with the ultimate goal of developing a new approach for site characterization. DAET has shown promising results at the laboratory scale for the study of nonlinear elasticity of Earth materials, detailing the full nonlinear elastic properties of the studied sample. We demonstrate the feasibility of DAET in situ and compare it to other methods (nonlinear resonance spectroscopy, wave amplitude dependence of propagation velocity, and wave distortion). Nonlinear elastic properties are characterized by DAET with the advantage of providing a local assessment compared to other methods, here at a depth of 4 m to 5 m. A vertical dynamic strain amplitude of 5×10^{-5} produces a relative change in compressional wave modulus of 6%. We measure an effective parameter of quadratic elastic nonlinearity of order -10^3, the same order of magnitude measured at the laboratory scale in rocks and in packs of unconsolidated glass beads. Hysteresis is observed in the variation in soil elasticity as a function of the instantaneous dynamic strain that evolves as the dynamic strain amplitude is increased from 9×10^{-7} to 5×10^{-5}.

1. Introduction

Strong ground motion occurs most frequently where low-velocity, soft sediments overlay hard rock. When seismic waves encounter low seismic velocity material, it increases wave amplitude due to conservation of momentum. In addition, standing waves can be generated with associated large amplitudes for resonant frequencies as a consequence of the layered structure of soil deposits. The effect of the local material elasticity on seismic wave frequency and amplitude is broadly known as the *site effect*. Seismic wave-induced ground motions can be either amplified or dissipated significantly relative to bedrock, and quasi-standing wave frequencies can be altered significantly due to the phenomena of nonlinear dissipation and "modulus reduction," respectively [e.g., *Field et al.*, 1997]. In situ observations [e.g., *Johnson et al.*, 2009] and numerous laboratory studies [*Stokoe et al.*, 1999; *Beresnev and Wen*, 1996; *Johnson and Jia*, 2005; *Brunet et al.*, 2008] confirm that sediments under dynamic wave loading produce wave amplitude-dependent, nonlinear, and hysteretic elastic behavior due to nonlinear contact mechanics.

Observations of nonlinear site effects are widespread, including from the 1994 Northridge earthquake [*Field et al.*, 1997, 1998; *Beresnev and Wen*, 1996], the 1994 Hyogoken Nanbu earthquake at Port Island, Kobe [*Aguirre and Irikura*, 1997], the 2001 *M* 6.8 Nisqually earthquake [*Frankel et al.*, 2002], the 2003 M_w 7.0 Miyagi-Oki earthquake [*Tsuda et al.*, 2006], the 1989 M_w 6.9 Loma Prieta Earthquake [*Rubinstein and Beroza*, 2004], the 1999 Chi-Chi, Taiwan, earthquake [*Roumelioti and Beresnev*, 2003], the 1994 M_w 8.2 Hokkaido Toho-oki earthquake [*Higashi and Sasatani*, 2000], as well as scores of others. In situ observations [e.g., *Field et al.*, 1997] show that the shear elastic modulus of soil can be reduced in more than half for strain amplitudes between 10^{-5} and 10^{-4} [*Johnson et al.*, 2009], consistent with laboratory measurements [*Beresnev and Wen*, 1996].

Laboratory measurements designed to extrapolate to various earthquake ground motions are a useful complement to field observations. Core samples are commonly used for laboratory measurements of elastic

nonlinear behavior [*Hardin and Drnevich*, 1972a, 1972b; *Ishihara*, 1996; *Seed et al.*, 1986]. A drawback in measuring properties from core for unconsolidated sediments is the fact that they are difficult to handle, and the soil studied in the laboratory is usually in a different compaction state than in the field. Since it is known that the elastic properties of unconsolidated soils depend on their compaction state [*Inserra et al.*, 2008; *Jia et al.*, 2011], the extrapolation of these laboratory results to field conditions is challenging and motivates the development of in situ characterization approaches.

Over the last decade, active in situ methods have been under development for probing elastic properties in the field [*Stokoe et al.*, 2001, 2008; *Menq et al.*, 2008; *Lawrence et al.*, 2008, 2009; *Johnson et al.*, 2009]. These methods involve strong shaking of the ground from a surface vibrator and measuring the response at the surface or in boreholes. In most cases, the vibration wave provides both the elastic disturbance and is also the measured quantity used to extract nonlinear elasticity and dissipation characteristics. Recently, a two-wave, or pump-probe method known as Dynamic Acoustoelastic Testing (DAET) has been under development, where a low-frequency vibration signal disturbs the material while a high-frequency low-amplitude wave probes the disturbance through multiple cycles of the low-frequency wave [*Renaud et al.*, 2009, 2011, 2012, 2013b]. Conceptually, this is identical to a laboratory acoustoelasticity measurement, where wave speed is measured as a sample is stressed [*Winkler and McGowan*, 2004; *Jaeger et al.*, 2007; *Bell*, 1992; *Bourbié et al.*, 1987]; however, in DAET the perturbation is a low-frequency wave, instead of a quasi-static load. A similar technique has been applied in situ to probe friable soils in field conditions [*Geza et al.*, 2001].

Our goal in this paper is to further develop the DAET approach to in situ conditions, with the ultimate goal of developing a new technique for evaluating site response. Here we report the use of DAET to characterize the nonlinear elastic behavior of a field site near Austin, Texas, USA. Our results demonstrate the feasibility of the technique in situ. We compare it to other in situ approaches, particularly nonlinear resonance spectroscopy, wave amplitude-dependent propagation velocity, and waveform distortion induced by nonlinear propagation. We show that indeed the method can be used to extract nonlinear elastic properties of a site. We also describe modifications that would improve its applicability.

2. Nonlinear Elasticity and Propagation of Elastic Waves

Nonlinear elasticity is defined as deviations from Hooke's law where the stiffness (or the elastic modulus) of a material depends on the applied strain (static or dynamic) and possibly on the strain rate. In metals and polymers, the relative variation in stiffness is of order 1–10 per unit strain. In cracked or granular media, cracks and contacts between grains can tremendously enhance relative stiffness variations that can be of order 1000 per unit strain, thus some orders of magnitude higher than in undamaged homogeneous solids. In a one-dimensional configuration, the equation of state relating the stress σ to the strain ϵ can be described as [*Zarembo and Krasil'nikov*, 1971; *Guyer and Johnson*, 2009]

$$\sigma = M_0 \left(\epsilon + \beta/2\,\epsilon^2 + \delta/3\,\epsilon^3 + H[\epsilon, \dot{\epsilon}]\right), \tag{1}$$

where M_0 is the linear elastic modulus, β and δ account for classical quadratic and cubic nonlinear elasticity, respectively, and the term $H[\epsilon, \dot{\epsilon}]$ accounts for hysteretic nonlinearity. In short, nonlinear elasticity causes the propagation of an elastic wave to be dependent on the wave amplitude. As a consequence, the wave speed and the attenuation depend on the amplitude of the elastic wave. Moreover, the waveform is distorted in the course of its propagation. Of importance here is the fact that elastic nonlinearity enables two elastic waves to interact with one another. If one wave has a large amplitude (pump) and the second has a small amplitude (probe), then the propagation velocity of the probe wave is modulated by the pump wave. Strain is generally considered as the main controlling parameter of nonlinear elasticity [*Guyer and Johnson*, 2009]; therefore, acceleration signals (see section 3.2).

3. Dynamic Acoustoelastic Testing In Situ

The purpose of DAET is to measure the wave amplitude dependence (or more generally stress dependence) of the compressibility of a material, i.e., the nonlinear portion of its equation of state (nonlinear elasticity). In DAET, we capitalize on the pump-probe concept: a material is probed simultaneously by two elastic waves, a low-frequency (LF) sine burst and a sequence of high-frequency (HF) pulses. A first source generates an LF

Figure 1. Photograph of the truck-mounted shaker ("T-Rex") used to generate the low-frequency wave (pump wave).

wave to dynamically stress a large volume of the propagation medium. A second source broadcasts the sequence of HF pulses in the studied area to determine the changes of time of flight (TOF) and amplitude of the HF pulses. Variations in the amplitude of the HF pulses correspond to changes of the HF attenuation induced by the LF forcing. Changes of TOF can be related to changes of elasticity of the soil. The nonlinear elastic parameters of the soil are extracted from the measured stress-induced variations in elasticity.

A unique advantage of DAET is the fact that it employs sinusoidal elastic waves, providing the means to probe the material under different stress states about the equilibrium state, producing both expansion and compression of the material as the LF signal sweeps over multiple sinusoidal cycles. As such, the method has been demonstrated to provide unique observation of complicated hysteretic behaviors and expansion-compression asymmetry in the laboratory [*Renaud et al.*, 2009, 2011, 2012, 2013b].

In summary, the physical idea that informs the development and use of DAET is that in a nonlinear material, two elastic waves from independently controlled sources interact with one another. The interaction carries information about the two independently controlled elastic waves, and it carries information about the nonlinear material in which these waves interact. The physical idea is sharpened in DAET, to focus on extracting information about the nonlinear material, by having the first of the independently controlled elastic wave to be of low frequency and large amplitude (the *pump* wave or LF wave) and having the second of the independently controlled elastic wave to be of high frequency and small amplitude (the *probe* wave or HF wave). Essentially, the probe wave detects the disturbance of the material brought about by the pump wave.

3.1. Experimental Configuration

The site chosen for this field application of DAET is located near Hornsby Bend (Austin, Texas, USA). The field had been ploughed in the preceding decades, leaving plough tillage (with topsoil and rocks) at the ground surface. The test site was prepared by removal of surface vegetation using a tiller. The top of the vegetation and topsoil was tilled and removed by hand with a shovel to reach native sandy silt at a depth of approximately 7 cm. The soil at this depth had a water content of 4 to 5% and a density (wet) of approximately 1900 kg/m^3 [*LeBlanc et al.*, 2012].

The LF source (pump), from a mobile hydraulic shaker dubbed *T-Rex* (Industrial Vehicles International Inc., Tulsa, USA), Figure 1, is a 4 m^2 square base plate that presses on the ground with a DC downward force of 267 kN (66.8 kPa). This base plate is driven vertically at 30 Hz during 0.7 s (21 periods) with AC force amplitudes that vary from 9 kN to 222 kN. Throughout the experiment, the downward force is greater than zero, i.e., the base plate does not lose contact with the ground.

A 30 cm diameter borehole was drilled to a depth of 3 m near the base plate of the T-Rex (x = 1.9 m and y = 1.2 m; see Figure 2). Two accelerometers (one-dimensional, AC135-1A, nominal sensitivity 0.5 V/g ±3%, ±10% frequency response 0.6–1500 Hz, Connection Technology Center Inc., Victor, USA) were installed at a depth of 4 m (detector 1) and 5 m (detector 2) to measure the vertical component of acceleration (Figure 2). The installation process involved boring a 3.8 cm diameter hole by hand auger to the required depth, alignment and installation of the accelerometer using a 6 m long PVC pipe, and backfill with native soil of the auger hole above the accelerometer. Backfilling was performed by placing auger material in the holes and using a rod to compact the soil. Care was taken to compact the backfilled soil to the same density as the in situ soil (evaluated by volume of auger material remaining). The uncertainty of the 1 m distance between the two accelerometers is ±1 cm. The precision of the distance between the base plate of the T-Rex and the accelerometers is ±5 cm. A HF vibratory source (Redpath Geophysics, Murphys, USA) was placed at 3 m depth. The HF source (probe) is a 13 cm diameter piston moving vertically (along z direction) and broadcasting HF pulses downward. It is driven with a sequence of 1 kHz short sine bursts with duration

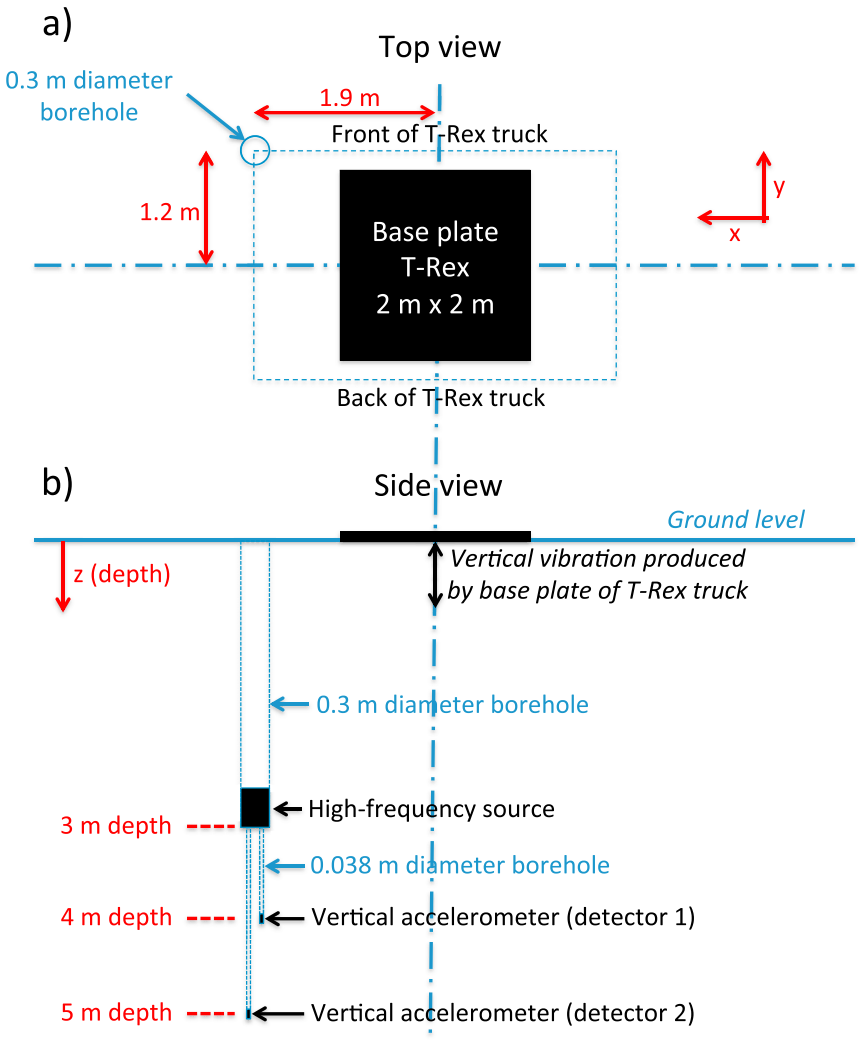

Figure 2. (a) Top view and (b) side view depicting the experimental configuration, the position of the T-Rex (LF source), and the measurement borehole with the HF source and the two buried accelerometers.

of 3 ms (three periods), repeated every 12.5 ms, at constant amplitude during the entire course of the experiments.

3.2. Signal Processing and Data Acquisition

The basic data sets are the acceleration time trains recorded on detectors 1 and 2 (Figure 2b). The output of the accelerometers is an analog voltage, and this is fed to a recording system at the surface which digitally converts the signal with a sampling period of $\tau_{\text{sample}} = 20$ μs. Each time train is split into (1) a LF part, found by Fourier analysis and band passing at 20 Hz $< f <$ 200 Hz and (2) a HF part, found by Fourier analysis and band passing at 700 Hz $< f <$ 5000 Hz. As an illustration, we show in Figure 3 a raw acceleration signal measured by the accelerometer at 4 m depth and its decomposition into LF and HF portions.

The resulting time trains, accelerations $\gamma_{\text{LF}}(t)$ and $\gamma_{\text{HF}}(t)$, are converted to displacements $u_{\text{LF}}(t)$ and $u_{\text{HF}}(t)$ by double time integration. Strains $\epsilon_{\text{LF}}(t)$ and $\epsilon_{\text{HF}}(t)$ are obtained using

$$\epsilon_{\text{LF}} = \left[u_{\text{LF 5m depth}}(t) - u_{\text{LF 4m depth}}(t)\right]/L, \tag{2}$$

$$\epsilon_{\text{HF}} = \frac{2\pi f_{\text{HF}}}{V_{\text{HF}}} \times u_{\text{HF}}(t), \tag{3}$$

where L, f_{HF}, and V_{HF} are the distance between the two buried detectors, the center frequency of the probe HF pulses, and the compressional wave speed measured with the probe HF pulses, respectively. While the

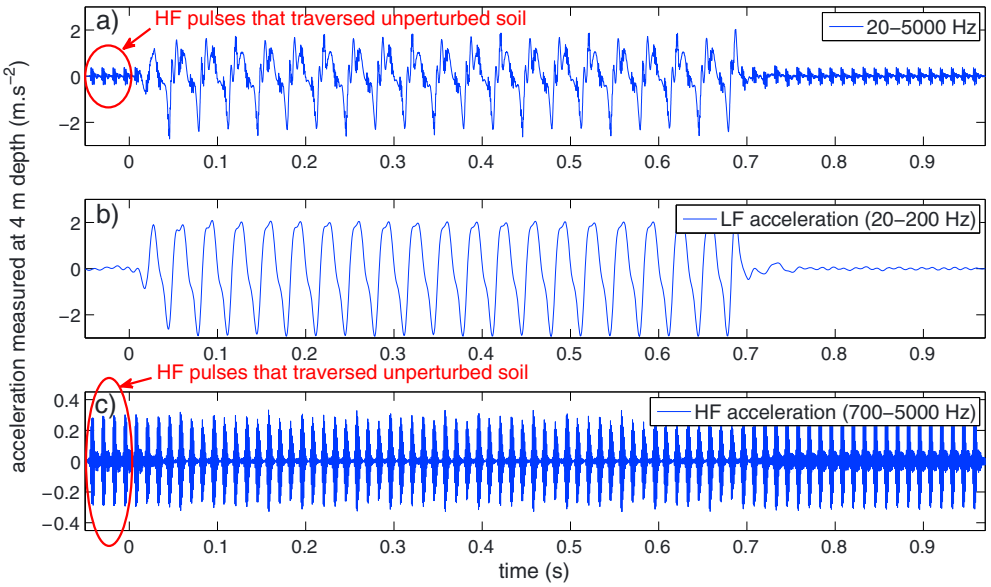

Figure 3. (a) Acceleration time signal measured by the accelerometer at 4 m depth. The LF source is driven with an AC force amplitude of 133 kN. (b) LF signal and (c) HF signal extracted by means of two band-pass frequency filtering with bands (20 Hz–200 Hz) and (700 Hz–5000 Hz), respectively.

calculation of the LF strain is exact by differentiation of the LF displacement measured by detectors 1 and 2 (the LF displacement field varies smoothly between 4 m and 5 m depth), the HF strain is estimated at detectors 1 and 2 assuming a monochromatic plane wave model. Figures 4a and 4b show the calculated time signals of the LF strain and the HF strain.

The HF source (probe) produces an estimated dynamic strain amplitude of 8.1×10^{-8} at detector 1 and 1.5×10^{-8} at detector 2, much smaller than dynamic strains generated by the LF source (base plate of the T-Rex) that range from 9×10^{-7} to 5×10^{-5} (see section 3.3). The amplitude of the HF signal at detector 2 decreases from that at detector 1 by a factor of 5.4 due to intrinsic absorption, scattering, and geometrical spreading of the wavefront. The first HF pulse in the sequence of HF pulses (Figure 3) propagates in undisturbed soil; it is used to establish that the time of flight from detector 1 to detector 2 is $t_0 = 1.86$ ms (obtained by using a cross-correlation method applied to signals received by the two accelerometers). It corresponds to a compressional velocity $V_{HF} = 538$ m/s $\pm$ 1% in undisturbed material.

In order for the results of a DAET experiment to have simple interpretation, we want the LF wave to establish a strain field that remains in place for a period of time long compared to the time during which the HF probe field encounters it, i.e., the time to travel from detector 1 to detector 2. The LF strain field has a period of $T_{LF} = 33.3$ ms, therefore 18 times larger than $t_0 = 1.86$ ms as required. The LF strain field ideally varies spatially only slightly in the region traversed by the HF pulses.

3.3. Experimental Protocol

The probe of the nonlinear properties of the soil is conducted with an elaborate experimental protocol. It consists of a reference run and a stepwise sequence of runs at finite LF source amplitude. The LF source (T-Rex truck) is driven successively at nominal peak force amplitudes of 9-18-9-36-9-67-9-133-9-222-9 kN. The corresponding LF strain amplitudes produced between the two buried accelerometers are given in Figure 5. A reference run at the lowest LF source amplitude (9 kN), interleaved between all runs at finite LF source amplitude, is applied to monitor potential slow evolution of the elastic properties of the site. We describe now the detailed experimental protocol.

1. The reference run.
   (a) The HF source is turned on and a HF pulse is broadcasted every 12.5 ms for approximately 1000 ms (Figures 3 and 4).
   (b) Using the lowest LF source amplitude, strain $\epsilon_0 = 9 \times 10^{-7}$, the LF source is turned on about 50 ms after the HF source is turned on and kept on for approximately 21 periods, about 700 ms. In this first

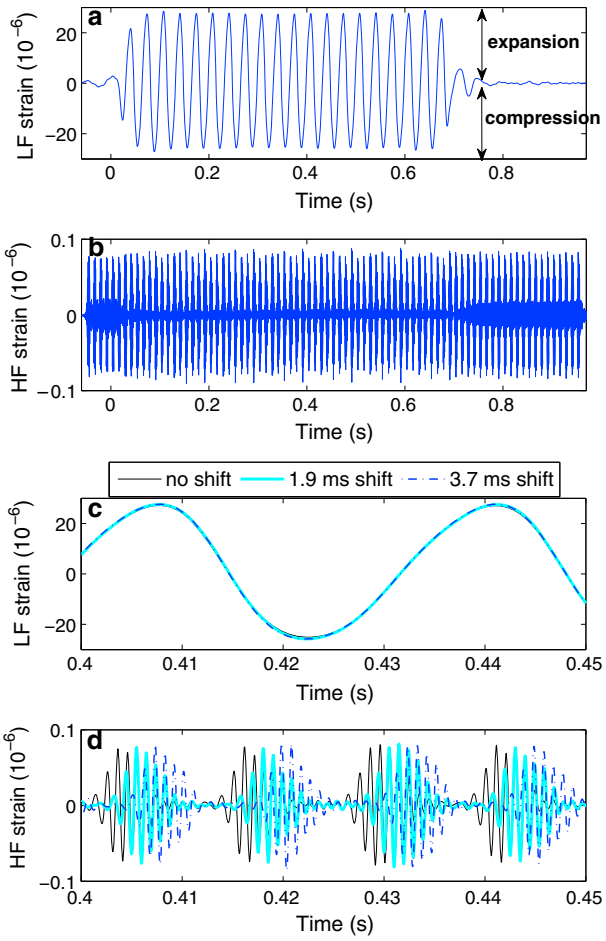

Figure 4. (a) LF strain measured between the two buried accelerometers as a function of time calculated from the LF acceleration signals measured at 4 m depth (Figure 3b) and 5 m depth using equation (2). The driving force amplitude of the LF source is 133 kN. (b) HF strain as a function of time estimated from the HF acceleration signal measured at 4 m depth (Figure 3c) using equation (3). (c and d) Enlargements of Figures 4a and 4b between 0.4 s and 0.45 s. (d) How the broadcast of the sequence of HF pulses is applied with three different delays (0, 1.9 ms, and 3.7 ms) with respect to the LF strain in order to probe soil under various discrete states of compression and expansion, at a given driving LF force amplitude. A positive LF strain produces an expansion of the soil while a negative LF strain represents a compressive strain.

run at ϵ_0 the phase of the initial LF pulse is set to zero relative to an arbitrary fiducial point in the sequence of HF pulses.

(c) With drive amplitude remaining at ϵ_0
   a. Steps (a) and (b) are repeated exactly with the single difference that the initial LF source is advanced in time by 1.9 ms relative to the fiducial point in the HF time train (Figure 4). This causes the HF pulses to traverse the soil under slightly different LF strain states.
   b. Steps (a) and (b) are repeated exactly with the single difference that the timing of the LF source is advanced in time by 3.7 ms relative to the fiducial point in the HF time train (Figure 4). Again, this ensures that the HF pulses traverse the soil under other slightly different LF strain states.

   Thus, a run has three *components* identified by the three settings of the time advance relative to the fiducial time. This first run, with the HF pulses crossing the 1 m thick region of soil between detectors 1 and 2 at many possible phases of the LF broadcast, is inserted throughout the measurement protocol to track the possible slow evolution of the elastic properties of the site.

2. Run at ϵ_1. Using LF source amplitude corresponding to $\epsilon_1 = 2 \times 10^{-6}$ steps (a)–(c) are repeated.
3. The reference run is repeated.
4. The measurement protocol continues. There are five runs at finite LF source amplitude, $\epsilon_1 = 2\times10^{-6}$ … $\epsilon_5 = 5\times10^{-5}$, and six reference runs, $\epsilon_0 = 9 \times 10^{-7}$ (Figure 5). All runs, reference and finite amplitude, have three components.

Note that the choice of 1.9 ms and 3.7 ms time shifts (Figure 4) was driven by experimental time considerations. Three components for each run (i.e., each LF driving amplitude) add significant time sampling improvement, but more components obtained with additional time shifts would further improve the results since the soil would be probed at higher time-sampling rate, i.e., at even more different states of dynamic compression and expansion.

3.4. Static Strain Field Between the Two Buried Detectors

The static strain field imposed by the DC downward force was estimated assuming an isotropically elastic solid half-space by the numerical evaluation of the analytical solution derived by *Becker and Bevis* [2004] (Figure 6). Based on *LeBlanc* [2013], we used 500 m/s and 250 m/s as average values on the site for the velocity of compressional and shear waves, respectively. We use the convention that a positive strain

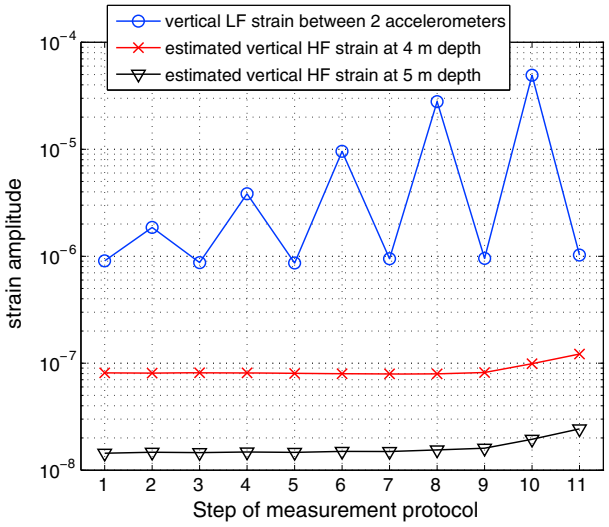

Figure 5. LF dynamic strain amplitude measured between the two buried detectors during the measurement protocol. The LF source (T-Rex truck) is driven successively at nominal peak force amplitudes of 9-18-9-36-9-67-9-133-9-222-9 kN. The HF dynamic strain amplitude is estimated at the two detectors; the driving amplitude of the LF source is constant through the entire measurement protocol. The reference runs at the lowest LF amplitude and the HF amplitudes show that only a small evolution of the elastic properties of the site occurred from runs 9 to 11 due to strong shaking generated by the T-Rex. The method to calculate the LF and HF strain amplitudes is detailed in section 3.2.

corresponds to an expansion of the material while a negative strain corresponds to a compression. The theoretically calculated DC strain field experienced by the region of soil probed by the HF pulses at $x = 1.9$ m (horizontal coordinate), $y = 1.2$ m (second horizontal coordinate), and $z = 4.5$ m (vertical coordinate) is $\epsilon_{xx} = +2.7 \times 10^{-6}$, $\epsilon_{yy} = +3.9 \times 10^{-6}$, $\epsilon_{zz} = -1.1 \times 10^{-5}$, $\epsilon_{xy} = -1.3 \times 10^{-6}$, $\epsilon_{zx} = -5.9 \times 10^{-6}$, and $\epsilon_{zy} = -3.7 \times 10^{-6}$. Finite element modeling using PyLith [*Aagaard et al.*, 2013] leads to similar strain values. The volumetric DC strain defined as $\epsilon_{xx} + \epsilon_{yy} + \epsilon_{zz}$ equals -4.1×10^{-6}, meaning that the soil traversed by the HF pulses experiences compression. Additionally, the lithospheric pressure (pressure on soil caused by the overlying weight of material from above) is of order 84 kPa which produces a DC vertical compressive strain of order $\epsilon_{zz} = -1.8 \times 10^{-4}$ (Figure 6). Therefore, the DC vertical strain induced by the lithospheric pressure between the two downhole detectors overwhelms the DC vertical strain produced by the T-Rex at this location ($\epsilon_{zz} = -1.1 \times 10^{-5}$) and hence determines the rest state of the soil. This means that the soil traversed by the HF pulses is under compression during the entire measurement.

3.5. Dynamic Pump Strain Field Between the Two Buried Detectors

The dynamic strain field produced at the largest AC force (222 kN) was calculated by the numerical evaluation of the analytical solution derived by *Jones et al.* [1998] (using a loss factor of 0.01). At this driving amplitude, the acceleration measured on the base plate of the T-Rex leads to a peak amplitude for the vertical dynamic displacement of 0.9 mm. This value is used to scale the numerical estimates detailed below. The base plate of the T-Rex is a square having a width of 2 m, and the LF wavelength for compressional waves is about 17 m. Therefore, the 30 Hz LF broadcast at the location of the two accelerometers corresponds to the case of the near field of a "short antenna"(size of the radiating source is much smaller than the wavelength). At the largest AC force, the LF strain field theoretically calculated between the two accelerometers ($x = 1.9$ m, $y = 1.2$ m, and $z = 4.5$ m) is such that the peak LF strain amplitudes are $\epsilon_{xx} = 2.7 \times 10^{-5}$, $\epsilon_{yy} = 3.1 \times 10^{-5}$, and $\epsilon_{zz} = 6.1 \times 10^{-5}$ (Figure 6). Thus, the largest component is the vertical LF strain ϵ_{zz}, and its sign is opposite to that of ϵ_{xx} and ϵ_{yy}. The corresponding volumetric LF strain amplitude is 3×10^{-6}; it has the same sign as the vertical LF strain ϵ_{zz}. Note that there exist shear strain components that are smaller than ϵ_{zz}. Additionally, we performed a finite difference time domain (FDTD) simulation for lossless elastic wave propagation (SimSonic) [*Bossy et al.*, 2005] and obtained a vertical LF strain amplitude ϵ_{zz} of 5.5×10^{-5}. The latter value is very close to that obtained with the analytical solution. Experimentally, we measured $\epsilon_{zz} = 4.9 \times 10^{-5}$ applying equation (2) (Figure 5) therefore in good agreement with numerical estimates.

In the remainder of the manuscript, we call *LF strain* the vertical component of the dynamic strain ϵ_{zz} produced by the base plate of the T-Rex between the two accelerometers, i.e., in the region probed by the HF pulses.

3.6. Data Processing and Analysis of DAET

The first data processing step is to determine the traveltime and attenuation of the HF pulses (probe) in order to observe how these quantities depend on the strength of the LF strain (pump) that the HF pulses experience. As noted, a HF pulse received at detector 1 goes on to detector 2, crossing

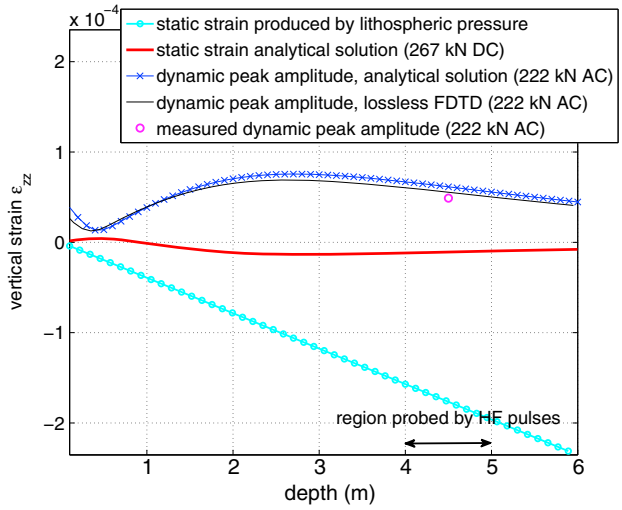

Figure 6. DC and AC vertical strain ϵ_{zz} experienced by the soil along the borehole (x = 1.9 m and y = 1.2 m) as a function of depth. The region of soil probed by the HF pulses between 4 m and 5 m depth is indicated by a double arrow. The DC vertical strain imposed by the 267 kN downward force is estimated with an analytical solution [*Becker and Bevis*, 2004]; it turns out to be smaller than the effect of lithospheric pressure. The AC vertical strain amplitude produced by the base plate of the T-Rex is estimated at the largest driving amplitude (222 kN) with two methods: numerical evaluation of an analytical solution [*Jones et al.*, 1998] and 3-D lossless FDTD simulation [*Bossy et al.*, 2005]. The AC vertical strain amplitude measured experimentally is in good agreement with the two numerical estimates.

L = 1 m, in t_0 = 1.86 ms. The LF strain modulates the properties of the material along the L path by a small amount. The resulting shift in the time to traverse L can be found from the cross correlation of the detected signal at detector 1 with the detected signal at detector 2. The cross correlation is carried out applying Tukey windows (ratio of the length of taper section is 5%) of width 4 ms which cover the first four periods of the HF pulses. Note that the duration of the HF pulses received at the two detectors is longer than that of the excitation waveform (3 ms) of the HF source because of the response of the HF source (ringing) and scattering. The typical lag/lead in the resulting cross correlation, when the time t_0 associated with crossing L at $\epsilon_{LF} = 0$ is removed, is of order 1% of t_0, i.e., of the same order as the time sampling rate, 20 μs. An interpolation scheme is used to sharpen the time resolution of the cross correlation [*Céspedes et al.*, 1995; *Renaud et al.*, 2011, 2012]. It is in this way that the data shown in Figure 7 are obtained. In Figure 7a the average LF strain experienced by the HF pulses during their propagation from detector 1 to detector 2 is plotted as a function of time. On this time train the arrival times of the HF pulses are indicated by open circles. This figure is constructed by overlaying the broadcasts from the three components of the run at LF source amplitude 133 kN.

The compressional wave modulus $M = \lambda + 2\mu$ is related to the compressional wave speed in an isotropic solid V_{HF} since $M = \rho V_{HF}^2$, ρ is the density, and λ and μ are the second-order elastic constants of Lamé. Remarking that $M = \rho V_{HF}^2 = \rho L^2/t^2$ and calculating the total differential for M leads to

$$\frac{\Delta M}{M_0} \approx 2\frac{\Delta L}{L_0} + \frac{\Delta \rho}{\rho_0} - 2\frac{\Delta t}{t_0} \tag{4}$$

The subscript 0 refers to the value in undisturbed material. Soil exhibits high elastic nonlinearity [*Field et al.*, 1997; *Beresnev and Wen*, 1996; *Johnson et al.*, 2009], and the relative variations in the HF traveltime $\Delta t/t_0$ are a few percent if the LF strain amplitude is of order 10^{-5} ($\Delta t/t_0$ <3.5%; see section 4.2). The dynamically induced distance change $\Delta L/L_0$ and density change $\Delta\rho/\rho_0$ between the two receivers have the same order of magnitude as the LF strain amplitude, which is at least 2 orders of magnitude smaller than the relative variations in the HF traveltime $\Delta t/t_0$. Thus, in our experiments, a change in arrival time of the HF pulses Δt lag/lead can be directly related to a variation in elastic modulus ΔM using

$$\frac{\Delta M}{M_0} \approx -2\frac{\Delta t}{t_0}. \tag{5}$$

It is $\Delta M/M_0$ that is plotted in Figure 7b as a function of time ($\Delta M/M_0$ is in percent).

The HF signals received at detectors 1 and 2 have different amplitudes A_1 and A_2, with the same basic shape (the amplitude of the normalized cross-correlation function is larger than 0.88). An amplitude is associated with each HF pulse by taking the maximum amplitude of the Fourier spectrum of the pulse found at a frequency close to 1 kHz (as above a 4 ms Tukey window that covers a pulse is used). From the HF attenuation

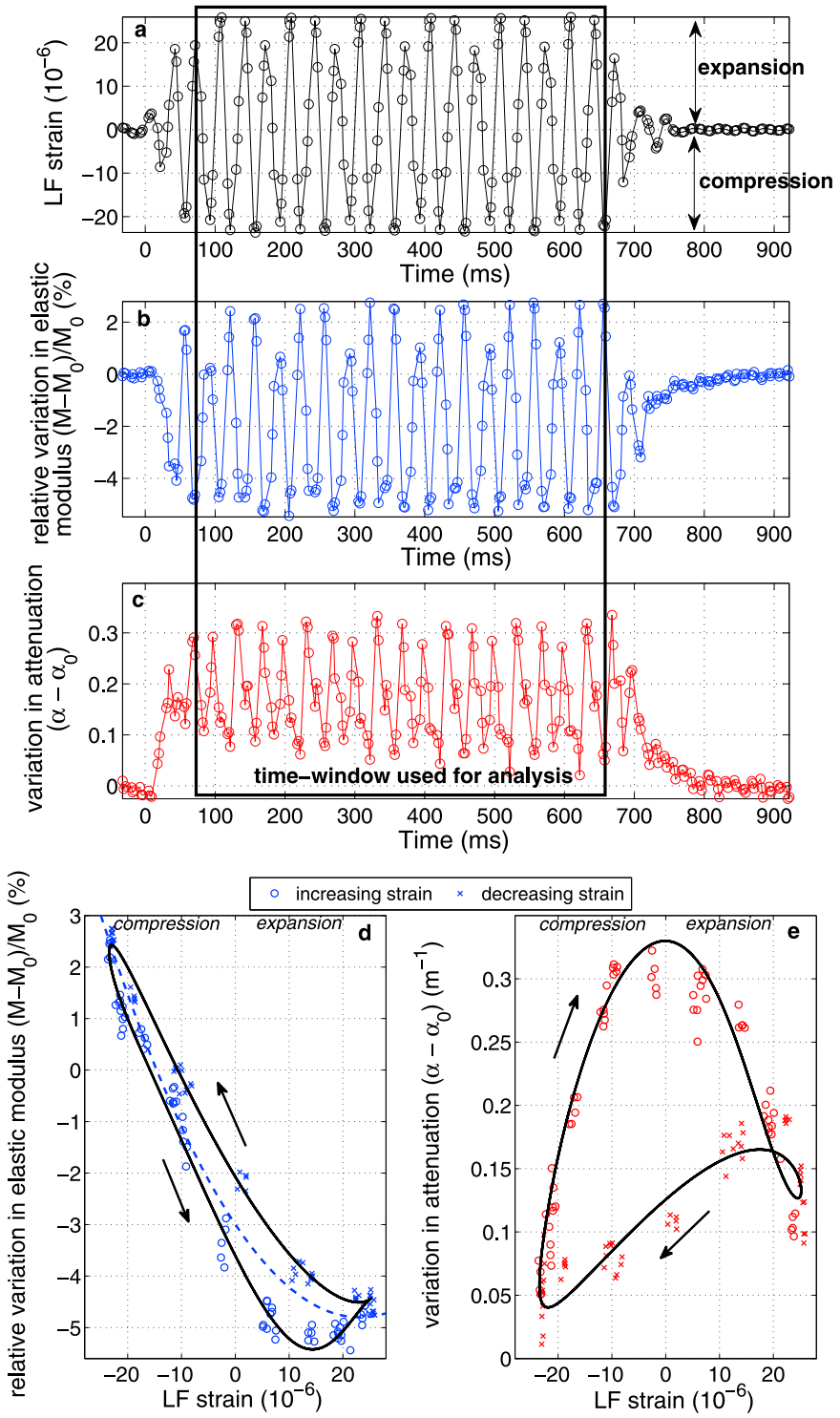

Figure 7. (a) LF strain experienced by the HF pulses, (b) variation in the elastic modulus M (from changes in HF arrival time), and (c) variation in the HF attenuation α as a function of time for a LF force amplitude of 133 kN. (d) Variation in the elastic modulus M (from changes in HF arrival time) and (e) variation in the HF attenuation α as a function of the LF strain for a LF force amplitude of 133 kN. The solid black lines indicate the interpolated (or up-sampled) behaviors using the result of the projection procedure. The dashed line in Figure 7d shows the parabolic fit applied to calculate the nonlinear elastic parameters (equation (7)). Each data point (open circle or cross) in these plots is associated with one HF pulse.

$\alpha(\epsilon_{LF})$ defined by $A_2(\epsilon_{LF}) = A_1(\epsilon_{LF}) \times \exp[-\alpha(\epsilon_{LF})L] \times D(L)$, where $D(L)$ accounts for diffraction effects, we find

$$\alpha(\epsilon_{LF}) = \frac{1}{L}\ln\left(\frac{A_1(\epsilon_{LF})}{A_2(\epsilon_{LF})}\right) + \frac{1}{L}\ln\left(D(L)\right) \tag{6}$$

Because geometrical spreading of the wavefront (wave diffraction) represented by $D(L)$ is not expected to be significantly changing as the LF strain amplitude is increased, the measured change in attenuation $\alpha(\epsilon_{LF}) - \alpha_0$ only accounts for changes in intrinsic absorption and scattering at 1 kHz. The HF attenuation in undisturbed material is α_0. The change in HF attenuation $\alpha(\epsilon_{LF}) - \alpha_0$ is reported in Figure 7c. The data shown in Figures 7a–7c can be captured more informatively in Figures 7d and 7e, where the modulus shift (Figure 7d) and the attenuation shift (Figure 7e) are plotted as a function of the LF strain ϵ_{LF}.

The elastic nonlinearity measured in soil is complicated as we shall see. We use two approaches that allow us to simplify the analysis but nonetheless interpret the nonlinear elastic response: a time domain approach and a frequency domain approach. In particular, note that these approaches do not provide a quantification of modulus-strain hysteresis.

3.6.1. Time Domain Approach

When the LF strain has reached a constant amplitude (at a given driving LF amplitude), the elastic response of soil is (approximately) in a meta stable steady state. During this period (between 80 ms and 650 ms; see Figure 7) it is possible to plot the relative variation in the elastic modulus as a function of the LF strain. Then we apply a parabolic fit to the relation between the relative variation in the elastic modulus $(M(\epsilon_{LF}) - M_0)/M_0$ and the LF strain ϵ_{LF}:

$$\frac{M(\epsilon_{LF}) - M_0}{M_0} \approx C_E + \beta_E\,\epsilon_{LF} + \delta_E\,\epsilon_{LF}^2. \tag{7}$$

β_E and δ_E are the classical nonlinear elastic parameters for quadratic and cubic elastic nonlinearity, respectively [e.g., *Johnson et al.*, 1996]. These parameters are defined for materials exhibiting classical nonlinear behavior due to atomic anharmonicity [*Zarembo and Krasil'nikov*, 1971]; however, it is commonly used to characterize materials whose nonlinear behavior is due to grain contacts, cracks, etc. C_E quantifies the DC offset of the modulation in the elastic modulus due to nonlinear material conditioning or hysteretic nonlinear elasticity [*Guyer and Johnson*, 2009]. For both changes in elasticity and attenuation, we also calculate the time-average variation over one LF period.

3.6.2. Frequency Domain Approach

In the nonlinear encounter between the probe and pump we expect the time of flight of the probe to be influenced by the timing of the LF strain, e.g., the shift in ΔM is modulated at frequency f_{LF} and multiples of f_{LF} [*Renaud et al.*, 2008; *Rivière et al.*, 2013]. The analysis of this modulation cannot be carried out by applying a conventional Fourier transform because the sampling period is not constant in a time trace $(M - M_0)/M_0$ composed of the combination of the three components in a run. To examine evidence of the probe carrying information about the time dependence of the pump, for each run, we carry out a projection analysis of the signals $d_M(t_i) = (M(t_i) - M_0)/M_0$, where t_i, $i = 1 \cdots N$ are the series of time points in the run. For example, from Figure 7b there are about 140 $(M - M_0)/M_0$ measurements over approximately 600 ms or 18 LF periods $T_{LF} = 1/f_{LF}$. The projection analysis, designed for sparse signal sets and/or irregularly sampled signals (see Appendix A), allows one to retrieve the modulation amplitude in a time trace $(M - M_0)/M_0$ at the pump frequency f_{LF} and multiples of f_{LF}. The projection procedure is also applied to the time traces of the LF strain $\epsilon_{LF}(t_i)$ (Figure 7a) and the attenuation change $(\alpha(t_i) - \alpha_0)$ (Figure 7c). Finally, it is possible to up-sample the result of the projection by using a time vector having a high sampling frequency, and the up-sampled time traces are used to plot interpolated behaviors for the time domain approach.

3.7. Analysis of LF Wave Propagation

The signal broadcast from the LF source (base plate of the T-Rex) is measured by an accelerometer mounted on the base plate and by the two accelerometers that are buried at 4 m and 5 m depths. However, measuring the compressional wave speed cannot be carried out with the LF signal, because the detectors are located in the near field of the LF source. Indeed, the size of the LF source (2 m) is close to the propagation distance to the buried detectors ($\approx$ 5 m). In this situation, compressional and shear (and Rayleigh) waves generated by the base plate of the T-Rex overlap spatially; therefore, the arrival of the LF signal at detectors 1 and 2 cannot be simply related to a pure compressional wave. Both shear and compressional waves contribute

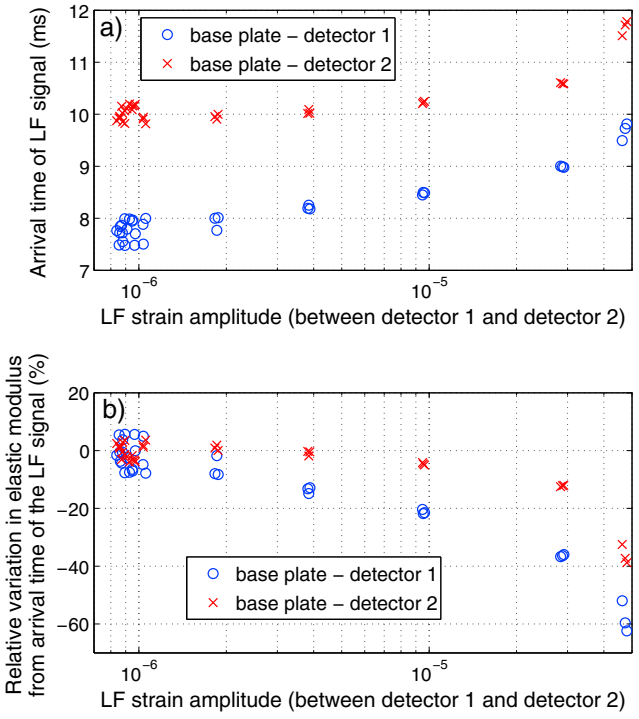

Figure 8. (a) Arrival time of the LF signal at the two buried accelerometers (time delay with respect to the LF signal measured by the accelerometer mounted on the base plate of the T-Rex) as a function of the LF strain amplitude. (b) Corresponding relative change in elasticity as a function of the LF strain amplitude derived from the relative change in arrival time of the LF signal.

to the soil motion recorded by the two buried accelerometers. Additionally, the determination of the propagation distance of the LF wave is problematic because the distance between the LF source and the buried detectors is close to the size of the LF source. Nonetheless, it is possible to convert a relative change in delay time of the LF signal recorded on the buried accelerometers with respect to the LF signal measured on the base plate of the T-Rex (by applying a cross-correlation method) to a relative change in elasticity as the LF driving amplitude is increased. However, as noted, the elastic modulus is not the compressional wave modulus (as in DAET; see equation (5)) because the arrival time of the LF signal cannot be attributed to a pure compressional wave. We will see in section 4.1 that the variations in arrival time of the LF signal are much larger than those observed with DAET; therefore, we must use the exact expression of equation (5), $\Delta M/M_0 = -\Delta t^2/t_0^2$.

4. Results

How does the nonlinear character of the material involved in this study make itself known in the observations that can be made? The pump modifies the material through which the probe propagates. So the probe is to be studied. But additionally, the pump interacts with itself. Consequently, we can look for evidence of the nonlinear elastic behavior of the material both in the received pump signals and in the received probe signals.

4.1. Pump

As noted previously, the pump signal is recorded by an accelerometer mounted on the base plate of the T-Rex as well as at the two downhole detectors. The times of flight, calculated using a cross-correlation method, between the LF acceleration signal at the base plate and the LF acceleration signal at detectors 1 and 2 (see Figure 3), are found. In Figure 8 the relative change in elastic modulus (derived from the relative increase in the arrival time of the LF signal) is plotted as a function of the LF strain as the AC driving force is increased from 9 to 222 kN, corresponding to a LF strain amplitude (between the two buried accelerometers) from 9×10^{-7} to 5×10^{-5}. At the largest AC driving force, an effective relative decrease in elastic modulus of 50% is observed. This observation accords with a variety of similar observations [*Johnson and Jia*, 2005; *Nazarov et al.*, 2010].

The frequency content of the pump signal $\epsilon_{LF}(t)$ may also be analyzed, since the progressive distortion of its waveform as it propagates [*Hamilton and Blackstock*, 1998] carries information about the nonlinear material properties. This method is commonly applied with a source able to broadcast a sine wave with very low harmonic distortion. Unfortunately, the waveform generated by seismic vibrators such as the T-Rex is significantly distorted [*Lebedev and Beresnev*, 2004]. In addition, the buried detectors are in the near field of the LF source. In this configuration, there exists no analytical solution to estimate nonlinear elastic parameters. Consequently, this method is not suitable to this experimental situation.

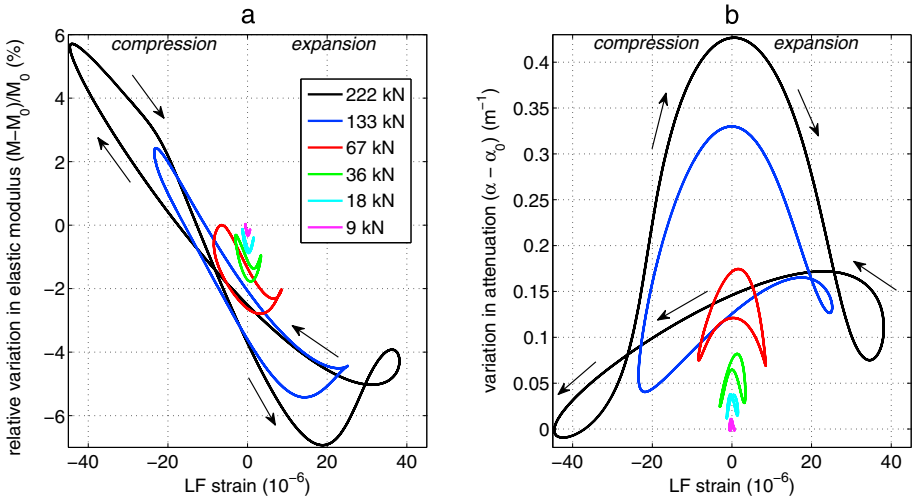

Figure 9. Up-sampled variation in (a) the compressional wave modulus M and (b) the HF attenuation α as a function of the LF strain, obtained as in Figure A1c using the results of the projection procedure. Behaviors for all six driving LF amplitudes are superimposed (only one response at the lowest LF amplitude is shown).

4.2. DAET

The probe signal is recorded at the two downhole detectors. A change in compressional wave modulus, deduced from the changes in time of flight between the detectors (equation (5)), is found to be a complicated function of the instantaneous LF strain. For six LF driving amplitudes (the reference run

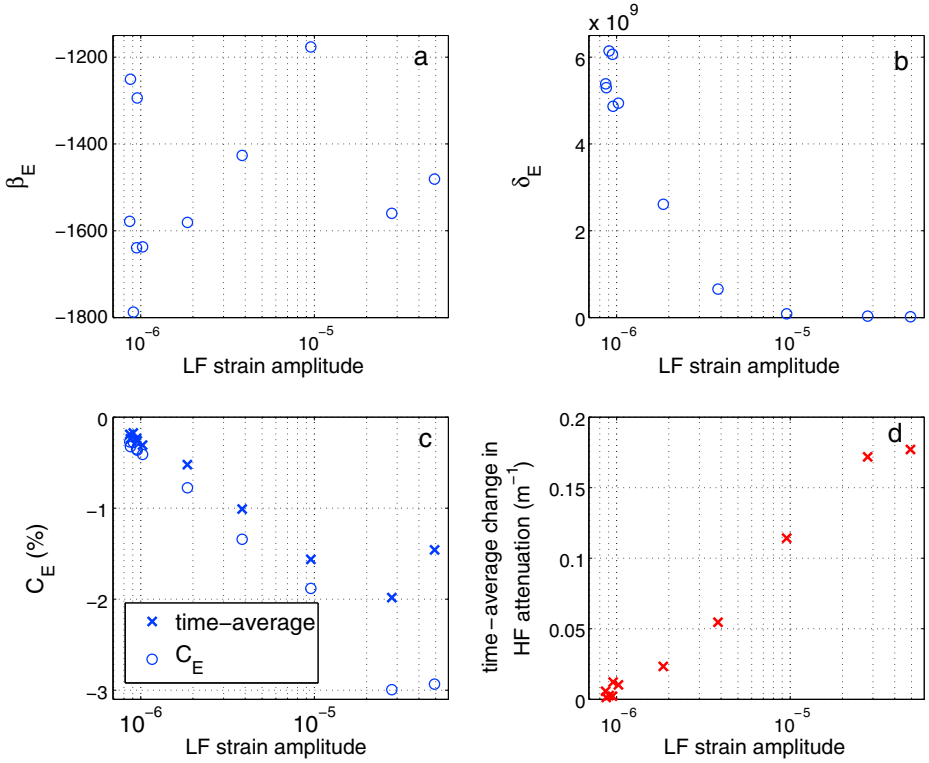

Figure 10. (a–c) Nonlinear elastic parameters measured with DAET and evaluated with the parabolic fit (equation (7)). Time-averaged variations in the compressional wave modulus M and the HF attenuation α as a function of the LF strain amplitude are shown in Figures 10c and 10d, respectively. The time-average change in elastic modulus has the same unity as C_E.

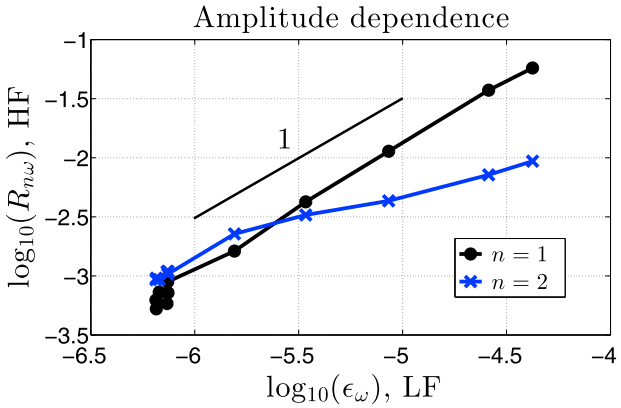

Figure 11. Amplitude of the modulation of the compressional wave modulus M obtained with the projection analysis at the LF driving frequency and at twice the LF driving frequency as a function of the LF strain amplitude (equation (A8)). $R_{1\omega}$ is the modulation amplitude at 30 Hz, and $R_{2\omega}$ is the modulation amplitude at 60 Hz (equation (A9)).

and five finite amplitudes) the up-sampled modulus shift and attenuation shift as a function of the instantaneous value of the LF strain ϵ_{LF} are shown in Figure 9. The results for all six LF strain amplitudes are plotted. In each panel the sense in which the hysteresis loops are traversed is indicated with arrows for the largest LF driving amplitude (222 kN).

In Figure 10 the nonlinear parameters estimated by applying a parabolic fit (equation (7)) are plotted as a function of the LF strain amplitude. A time-average measure of the modulus shift and attenuation shift for each LF strain amplitude is also provided by averaging over the instantaneous values of the LF strain (during one LF period). The six reference runs at the lowest LF amplitude (AC driving force = 9 kN) produced essentially the same result and suggests that there was little unrecoverable change in the elastic state of the material during the course of the experiment. The HF wave strain amplitude and the HF wave speed in undisturbed soil remain constant during the experiment. From the time-averaged variation, we see that there is an average modulus shift to lower modulus and an average attenuation shift to larger attenuation, which become larger as the magnitude of the LF strain increases. Unsurprisingly, the average change in modulus experienced by the probe behaves qualitatively like the change in modulus experienced by the LF broadcast (Figure 8). β_E shows a fairly constant value of $-1500 \pm 15\%$, whereas δ_E decreases tremendously from 6×10^9 to 2×10^7 as the LF strain amplitude increases from 10^{-6} to 5×10^{-5}.

The dynamic component of the change in modulus (the difference between the instantaneous modulus and the average modulus) is a complicated function of the instantaneous LF strain. To look into the behavior of this part of the modulus we turn to the decomposition provided by the projection analysis. In Figure 11 we show the modulation amplitudes at f_{LF} and $2f_{\mathrm{LF}}$, $R_{1\omega}$ and $R_{2\omega}$ (equation (A9)), as a function of ϵ_ω, the LF strain amplitude experienced by the HF pulses. The amplitude $R_{1\omega}$ scales with ϵ_ω. The amplitude $R_{2\omega}$ appears to scale approximately as a power of ϵ_ω that is less than 1. The nonlinear parameter β_E can be estimated by applying a linear fit to the relation between the modulation amplitude at f_{LF} ($R_{1\omega}$) and the LF strain [*Renaud et al.*, 2008; *Rivière et al.*, 2013]. This leads to $\beta_E = -1240$ and thus accords with values calculated applying a parabolic fit in the plots of instantaneous changes in elastic modulus versus instantaneous LF strain (Figures 7d and 10). The linear fit applied to the LF amplitude dependence of $R_{1\omega}$ (Figure 11) provides a more accurate estimate of β_E because it is not affected by the hysteresis loops (Figure 7d). The measured scaling between the modulation of the elastic modulus sensed by the probe at f_{LF} and the LF strain amplitude can be described by classical nonlinear elasticity (β_E), but this is not the case for the modulation at $2f_{\mathrm{LF}}$ ($R_{2\omega}$ in Figure 11). Indeed, classical cubic nonlinearity (δ_E) predicts a power law with a scaling exponent of 2, instead of less than 1 as found experimentally. The slope of less than 1 in Figure 11 is consistent with the fact that the nonlinear parameter δ_E decreases as the LF strain amplitude increases (Figure 10b).

In summary two qualities are conferred on the probe wave as it propagates through the material; it moves more slowly, experiencing the softening of the material caused by the pump, and it acquires an ω_{LF} and $2\omega_{\mathrm{LF}}$ components by coupling to the pump. In this way the probe reveals important information about the nonlinear character of the material.

5. Discussion

5.1. Comparison With Lab Measurements

The estimation of the nonlinear elastic parameter β_E with the time domain and frequency domain approaches from DAET leads to values of order -10^3, the same order of magnitude as those measured at the laboratory scale applying DAET and other techniques in room-dry rocks [*Guyer and Johnson*, 2009; *Renaud et al.*, 2011, 2013a; *Winkler and McGowan*, 2004] and in unconsolidated glass bead packs [*Brunet et al.*, 2008]. As

in rocks at the laboratory scale [*Renaud et al.*, 2012, 2013b; *Rivière et al.*, 2013], the nonlinear elastic parameter δ_E is not constant; it decreases (in absolute value) as the LF strain amplitude increases. Thus, classical cubic elastic nonlinearity (δ_E) is not suitable to describe the nonlinear elastic response of soil. As observed in laboratory studies, the LF strain produces a time-average reduction of the elastic modulus in soil (Figure 10), and the higher the LF strain amplitude, the larger the softening. A reduction of the elastic modulus of 2% is observed for a LF strain amplitude of order 10^{-5}. Laboratory measurements in rocks show time-average changes in modulus of the same order of magnitude [*Renaud et al.*, 2013a, 2011].

5.2. Different Information Carried by the Pump and the Probe

The time-average change in elastic modulus measured with the pump is of order 10% (Figure 8) while the probe experiences an average change in elastic modulus of order 1% (Figure 10c). This difference comes from the fact that the probe carries local information on the effect of the pump on the material. On the contrary the pump signal measured at the two downhole detectors carries information on the interaction between the pump wave and the material, from the LF source to the detectors. The effect of interaction between the pump wave and the material on the propagation of the pump wave is cumulative. Since the LF strain close to the LF source is an order of magnitude larger than at the two downhole detectors (due to diffraction loss), the average change in elastic modulus measured by the pump is expected to be larger than that measured by the probe at 5 m away from the LF source. Additionally, the relative change in arrival time of the LF signal at 4 m or 5 m depths (as the LF strain amplitude increases) cannot be related to a relative change in the compressional wave modulus $M = \lambda + 2\mu$ as in DAET. Indeed, the buried accelerometers are situated in the near field of the LF source; therefore, the LF motion measured by the accelerometers is the result of the compressional, shear, and Rayleigh wave fields generated by the LF source that coexist spatially at this location as noted previously. As a result the information carried by the pump and the probe is different and can only be compared qualitatively.

5.3. Comparison With Nonlinear Resonance Spectroscopy

Our in situ measurements in soil can be compared to observations made applying nonlinear resonance spectroscopy in situ to soil employing the same vibrator source [*Johnson et al.*, 2009]. This method allows one to measure a time-average change in elasticity. The authors reported a reduction of the shear elastic modulus μ to about 56% of its value at rest, for a pump frequency and strain amplitude similar to our study. The time-average reduction in elastic modulus is therefore significantly larger than what we observed. When applying DAET in our study, the base plate of the T-Rex is driven vertically instead of transversally in the work by *Johnson et al.* [2009] where a shear pump wave is generated. Thus, differences between our results and those by *Johnson et al.* [2009] may be due to the different nature of the pump strain. The shear modulus μ may vary more under the effect of a shear strain than under the effect of a volumetric strain having the same amplitude. This would explain why the relative reduction in soil modulus reported by *Johnson et al.* [2009] is larger than what we observed. Future DAET experiments could employ the T-Rex driven transversally in order to generate a shear pump wave; then one should be able to compare the results to the work by *Johnson et al.* [2009].

5.4. Current Limitations and Future Improvements

A limitation of the current setup is the fact that the soil must be removed to place the HF source and the two detectors in the borehole. Therefore, the compaction inside and outside the borehole may be different and alter the observations. An improvement of the method would be to use two (or more) boreholes, one containing the HF source and the other(s) containing one or more detectors. The LF source would be therefore placed in between the two boreholes, as the setup originally developed for medical ultrasound [*Renaud et al.*, 2008]. Moving the HF source and detector vertically in the boreholes would enable one to probe the soil at different depths. Indeed, the nonlinear elasticity of soil is expected to be depth dependent, this being a consequence of the lithospheric pressure. Ultimately, DAET measurements could include the broadcast and analysis of the probe at multiple depths, providing the means for nonlinear elasticity of soil to be assessed at different depths.

Finally, applying DAET with three different configurations for the probe (compressional wave and shear wave, different polarization of shear wave, and different propagation direction with respect to the LF pump field) as in conventional lab acoustoelastic testing [*Winkler and McGowan*, 2004] could provide estimates of the three third-order elastic constants, required to describe classical quadratic nonlinear elasticity

in an isotropic solid material [*Zarembo and Krasil'nikov*, 1971; *Guyer and Johnson*, 2009; *Hamilton and Blackstock*, 1998].

6. Conclusions

A methodology termed Dynamic Acoustoelastic Testing to infer nonlinear elastic properties of materials was tested in the field using a large shaker source known as T-Rex, which heretofore had only been attempted on laboratory rock specimens. Even in a relatively soft soil, clear identification of the HF probe and LF pump signals was made for a range of LF source amplitude corresponding to soil dynamic strain levels of 9×10^{-7} to 5×10^{-5} at 4.5 m depth. Despite an experimental arraignment that may have introduced soil disturbance, the technique appears viable for determining nonlinear elastic parameters. Challenges remain to develop the technique for a broader application to deeper sediments and higher strains for determination of wave amplitude dependence of bulk and shear moduli. Clearly, in situ measurement of the nonlinear site response is advantageous to provide optimal information for prediction of strong ground motion at a site. DAET is a method that holds promise for doing just that.

Appendix A: Projection Analysis

A projection analysis, designed for sparse signal sets and/or irregularly sampled signals, employs a complete set of functions that are constructed to be orthonormal on the sparse signal set [*Rivière et al.*, 2013]. These functions are

$$S_n(t_i) = q_n \sin(n\,\omega_{\mathrm{LF}}\,t_i), \quad i = 1 \cdots N, \tag{A1}$$

$$C_n(t_i) = r_n \cos(n\,\omega_{\mathrm{LF}}\,t_i), \quad i = 1 \cdots N, \tag{A2}$$

$$< S_n S_m >= \delta_{nm}\,, \tag{A3}$$

$$< C_n C_m >= \delta_{nm}\,, \tag{A4}$$

$$< S_n C_m >= 0\,, \tag{A5}$$

where $\omega_{\mathrm{LF}} = 2\pi f_{\mathrm{LF}}$ and $n = 1, 2, \cdots$. Practically, q_n and r_n are found using the numerical Gram-Schmidt process [*Rivière et al.*, 2013]. We project the sparse signal $d_M = (M - M_0)/M_0$ (Figure 7b) on the series of orthonormal functions and we have

$$a_n =< S_n\, d_M >= \sum_{i=1}^{N} S_n(t_i)\, d_M(t_i), \tag{A6}$$

$$b_n =< C_n\, d_M >= \sum_{i=1}^{N} C_n(t_i)\, d_M(t_i), \tag{A7}$$

and

$$d_M^p(t_i) = \sum_{n=1}^{N} a_n S_n(t_i) + \sum_{n=1}^{N} b_n C_n(t_i), \tag{A8}$$

i.e., a_n (respectively, b_n) is the amplitude with which d_M carries the time structure of S_n (respectively, C_n). In this expansion of d_M the sum on n goes to a practical limit, N. To characterize the presence of frequency $n\omega_{\mathrm{LF}}$ in d_M we use the amplitudes

$$R_{n\omega} = \sqrt{(a_n q_n)^2 + (b_n r_n)^2}. \tag{A9}$$

The projection procedure is also used on the LF strains $\epsilon_{\mathrm{LF}}(t_i)$ found as in Figure 7a. We write

$$\epsilon_{\mathrm{LF}}^p(t_i) = \sum_{n=1}^{N} g_n S_n(t_i) + \sum_{n=1}^{N} h_n C_n(t_i), \tag{A10}$$

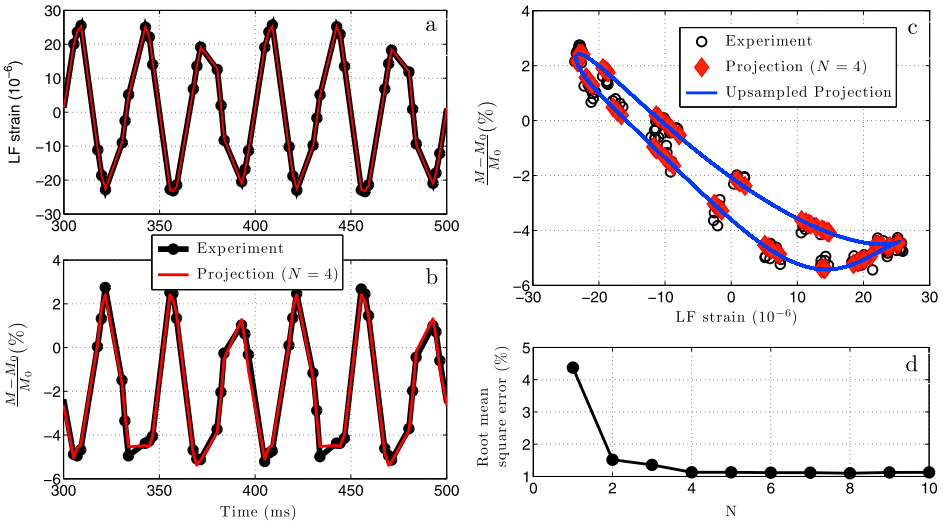

Figure A1. (a) LF strain as a function of time, exemplary result of the projection procedure (equation (A10)). (b) Relative modulus variation as a function of time, exemplary result of the projection procedure (equation (A8)). (c) Relative variation in elastic modulus as a function of the LF strain, comparison between raw experimental data, signal obtained by the projection procedure, and up-sampled signal after decomposition. (d) Root-mean-square error of the difference between the result of the projection analysis and the experimental data as a function of the order N of the decomposition. The driving LF force amplitude is 133 kN.

where g_n and h_n are equivalent to a_n and b_n in equation (A8). As an illustration of signal construction using the projection procedure we show, Figure A1, (a) a time segment of $\epsilon_{\mathrm{LF}}(t_i)$ as in Figure 7a and its reconstruction $\epsilon^p_{\mathrm{LF}}(t_i)$ as in equation (A10), (b) a time segment of $d_M(t_i)$ as in Figure 7b and its reconstruction $d^p_M(t_i)$ as in equation (A8), and (c) the values of $d_M(\epsilon_{\mathrm{LF}})$ as in Figure 7d, the reconstruction $d^p_M(\epsilon^p_{\mathrm{LF}})$ obtained from Equations A8 and A10 and an up-sampled version of the reconstruction. Finally, Figure A1d shows the root-mean-square error between experimental data $d_M(t_i)$ and the projection result $d^p_M(t_i)$ for different values of N. It is shown that $N > 4$ does not further improve the decomposition of the signal. Similar trend is found for the LF strain signal, and therefore, $N = 4$ is chosen for both LF and HF signals.

Acknowledgments

We gratefully acknowledge the support of the U.S. Department of Energy, Office of Basic Energy Research and the funding for the experiment by Terry Rust and Larry Goen of Los Alamos National Laboratory. We thank Farn-Yuh Menq (University of Texas) for data acquisition support. Thanks to Bruce Redpath for the design and installation of the high-frequency sources and receivers. We also thank Major Matthew LeBlanc and Captain Allen Branco (University of Texas) for assistance on installation of sensors and their field support during the course of the experiment. Finally, we thank Didier Cassereau for his help with SimSonic simulations.

References

Aagaard, B., M. Knepley, and C. Williams (2013), A domain decomposition approach to implementing fault slip in finite-element models of quasi-static and dynamic crustal deformation, *J. Geophys. Res. Solid Earth*, *118*, 3059–3079, doi:10.1002/jgrb.50217.

Aguirre, J., and K. Irikura (1997), Nonlinearity, liquefaction, and velocity variation of soft soil layers in Port Island, Kobe, during the Hyogo-Ken Nanbu earthquake, *Bull. Seismol. Soc. Am.*, *87*(5), 1244–1258.

Bell, F. (1992), *Engineering Properties of Soils and Rocks*, 3rd ed., pp. 1–345, Butterworth-Heinemann, Oxford, U. K.

Becker, J. M., and M. Bevis (2004), Love's problem, *Geophys. J. Int.*, *156*(2), 171–178.

Beresnev, I., and K.-L. Wen (1996), Nonlinear soil response—A reality?, *Bull. Seismol. Soc. Am.*, *86*(6), 1964–1978.

Bossy, E., F. Padilla, F. Peyrin, and P. Laugier (2005), Three-dimensional simulation of ultrasound propagation through trabecular bone structures measured by synchrotron microtomography, *Phys. Med. Biol.*, *50*(23), 5545–5556.

Bourbié, T., O. Coussy, and B. Zinszner (1987), *Acoustics of Porous Media*, pp. 1–334, Institut Français du Ptrole, Paris, France.

Brunet, T., X. Jia, and P. Johnson (2008), Transitional nonlinear elastic behaviour in dense granular media, *Geophys. Res. Lett.*, *35*, L19308, doi:10.1029/2008GL035264.

Céspedes, I., Y. Huang, J. Ophir, and S. Spratt (1995), Methods for estimation of subsample time delays of digitized echo signals, *Ultrason. Imaging*, *17*, 142–171.

Field, E., P. Johnson, I. Beresnev, and Y. Zeng (1997), Nonlinear ground-motion amplification by sediments during the 1994 Northridge earthquake, *Nature*, *390*(6660), 599–602.

Field, E., Y. Zeng, P. Johnson, and I. Beresnev (1998), Nonlinear sediment response during the 1994 Northridge earthquake: Observations and finite source simulations, *J. Geophys. Res.*, *103*(B11), 26,869–26,883.

Frankel, A., D. Carver, and R. Williams (2002), Nonlinear and linear site response and basin effects in Seattle for the M 6.8 Nisqually, Washington, earthquake, *Bull. Seismol. Soc. Am.*, *92*(6), 2090–2109.

Geza, N., G. Egorov, Y. Mkrtumyan, and V. Yushin (2001), Instantaneous variations in velocity and attenuation of seismic waves in a friable medium in situ under pulsatory dynamic loading: An experimental study, *Russ. Geol. Geophys.*, *42*(7), 1079–1087.

Guyer, R., and P. Johnson (2009), *Nonlinear Mesoscopic Elasticity*, pp. 1–396, Wiley-VCH Verlag GmbH and Co. KGaA, Weinheim, Germany.

Hamilton, M., and D. Blackstock (1998), *Nonlinear Acoustics: Theory and Applications*, pp. 1–455, Acad. Press, New York.

Hardin, B., and V. Drnevich (1972a), Shear modulus and damping in soil: Measurement and parameter effects, *J. Soil Mech. Found. Div.*, *98*(6), 603–624.

Hardin, B., and V. Drnevich (1972b), Shear modulus and damping in soil: Design equations and curves, *J. Soil Mech. Found. Div.*, *98*(7), 667–692.

Higashi, S., and T. Sasatani (2000), Nonlinear site response in Kushiro during the 1994 Hokkaido Toho-oki earthquake, *Bull. Seismol. Soc. Am.*, *90*(4), 1082–1095.
Inserra, C., V. Tournat, and V. Gusev (2008), Characterization of granular compaction by nonlinear acoustic resonance method, *Appl. Phys. Lett.*, *92*, 191,916, doi:10.1063/1.2931088.
Ishihara, K. (1996), *Soil Behaviour in Earthquake Geotechnics*, pp. 1–360, Oxford Univ. Press, Oxford, U. K.
Jaeger, J., N. Cook, and R. Zimmerman (2007), *Fundamentals of Rock Mechanics*, 4th ed., pp. 1–488, Wiley, Hoboken, N. J.
Jia, X., T. Brunet, and J. Laurent (2011), Elastic weakening of a dense granular pack by acoustic fluidization: Slipping, compaction and aging, *Phys. Rev. E*, *84*, 020,301, doi:10.1103/PhysRevE.84.020301.
Johnson, P., and X. Jia (2005), Nonlinear dynamics, granular media and dynamic earthquake triggering, *Nat. Lett.*, *437*(6), 871–874.
Johnson, P., B. Zinszner, and P. Rasolofosaon (1996), Resonance and elastic nonlinear phenomena in rock, *J. Geophys. Res.*, *101*(B5), 11,553–11,564.
Johnson, P., P. Bodin, J. Gomberg, F. Pearce, Z. Lawrence, and F.-Y. Menq (2009), Inducing in situ, nonlinear soil response applying an active source, *J. Geophys. Res.*, *114*, B05304, doi:10.1029/2008JB005832.
Jones, D. V., D. Le Houedec, A. T. Peplow, and M. Petyt (1998), Ground vibration in the vicinity of a moving harmonic rectangular load on a half-space, *Eur. J. Mech. - A/Solids*, *17*(1), 153–166.
Lawrence, Z., P. Bodin, C. Langston, F. Pearce, J. Gomberg, P. Johnson, F.-Y. Menq, and T. Brackman (2008), Induced dynamic nonlinear ground response at Garner Valley, California, *Bull. Seismol. Soc. Am.*, *98*(3), 1412–1428.
Lawrence, Z., P. Bodin, and C. Langston (2009), *In Situ Measurements of Nonlinear and Nonequilibrium Dynamics in Shallow, Unconsolidated Sediments*, 1650–1670, vol. 99.
Lebedev, A. V., and I. A. Beresnev (2004), Nonlinear distortion of signals radiated by vibroseis sources, *Geophysics*, *69*(4), 968–977.
LeBlanc, M. (2013), Field measurement of the linear and nonlinear constrained moduli of granular soil, PhD thesis, Univ. of Texas, Austin, Tex.
LeBlanc, M., K. I. Stokoe, A. I. Branco, and R. Lee (2012), Field determination of linear and nonlinear constrained moduli of soils using large mobile shakers, paper presented at 15th WCEE, Lisbon, Portugal.
Menq, F.-Y., K. I. Stokoe, K. Park, B. Rosenblad, and B. Cox (2008), Performance of mobile hydraulic shakers at nees@UTexas for earthquake studies, paper presented at 14th World Conference of Earthquake Engineering, pp. 1–8, Beijing, China, October 12-17.
Nazarov, V., A. Kolpakov, and A. Radostin (2010), Self-action of ultrasonic pulses in a marble rod, *Acoust. Phys.*, *56*(5), 632–636.
Renaud, G., S. Callé, J.-P. Remenieras, and M. Defontaine (2008), Exploration of trabecular bone nonlinear elasticity using time-of-flight modulation, *IEEE Trans. UFFC*, *55*(7), 1497–1507.
Renaud, G., S. Callé, and M. Defontaine (2009), Remote dynamic acoustoelastic testing: Elastic and dissipative acoustic nonlinearities measured under hydrostatic tension and compression, *Appl. Phys. Lett.*, *94*, 011,905, doi:10.1063/1.3064137.
Renaud, G., M. Talmant, S. Callé, M. Defontaine, and P. Laugier (2011), Nonlinear elastodynamics in micro-inhomogeneous solids observed by head-wave based dynamic acoustoelastic testing, *J. Acoust. Soc. Am.*, *130*(6), 3583–3589.
Renaud, G., P.-Y. Le Bas, and P. A. Johnson (2012), Revealing highly complex elastic nonlinear (anelastic) behavior of Earth materials applying a new probe: Dynamic acoustoelastic testing, *J. Geophys. Res.*, *117*, B06202, doi:10.1029/2011JB009127.
Renaud, G., J. Rivière, S. Haupert, and P. Laugier (2013a), Anisotropy of dynamic acoustoelasticity in limestone, influence of conditioning, and comparison with nonlinear resonance spectroscopy, *J. Acoust. Soc. Am.*, *133*(6), 3706–3718.
Renaud, G., J. Rivière, P.-Y. Le Bas, and P. Johnson (2013b), Hysteretic nonlinear elasticity of Berea sandstone at low-vibrational strain revealed by dynamic acousto-elastic testing, *Geophys. Res. Lett.*, *40*, 715–719, doi:10.1002/grl.50150.
Rivière, J., G. Renaud, R. Guyer, and P. Johnson (2013), Pump and probe waves in dynamic acousto-elasticity: Comprehensive description and comparison with nonlinear elastic theories, *J. Appl. Phys.*, *114*, 054,905, doi:10.1063/1.4816395.
Roumelioti, Z., and I. Beresnev (2003), Stochastic finite-fault modeling of ground motions from the 1999 Chi-Chi, Taiwan, earthquake: Application to rock and soil sites with implications for nonlinear site response, *Bull. Seismol. Soc. Am.*, *93*(4), 1691–1702.
Rubinstein, J., and G. Beroza (2004), Evidence for widespread nonlinear strong ground motion in the Mw 6.9 Loma Prieta earthquake, *Bull. Seismol. Soc. Am.*, *94*(5), 1595–1608.
Seed, H., R. Wong, I. Idriss, and K. Tokimatsu (1986), Moduli and damping factors for dynamic analyses of cohesionless soils, *J. Geotech. Eng.*, *112*(11), 1016–1032.
Stokoe, K., M. Darendeli, R. Andrus, and L. Brown (1999), Dynamic soil properties: Laboratory, field and correlation studies, in *Proceedings, Second International Conference on Earthquake Geotechnical Engineering*, vol. 3, pp. 811–845, A. A. Balkema, Rotterdam and Brookfield, Netherlands.
Stokoe, K., P. Axtell, and E. Rathje (2001), Development of an in situ method to measure nonlinear soil behavior, paper presented at Third International Conference on Earthquake Resistant Engineering Structures, ERES2001, Malaga, Spain, 4–6 Sept.
Stokoe, K. I., F.-Y. Menq, S. Wood, K. Park, B. Rosenblad, and B. Cox (2008), Experience with nees@UTexas large-scale mobile shakers in earthquake engineering studies, in *Proceedings of the Third International Conference on Site Characterization (ISC'3)*, pp. 1–6, Taipei, Taiwan, 1–4 April.
Tsuda, K., J. Steidl, R. Archuleta, and D. Assimaki (2006), Site-response estimation for the 2003 Miyagi-Oki earthquake sequence considering nonlinear site response, *Bull. Seismol. Soc. Am.*, *96*(4A), 1474–1482.
Winkler, K., and L. McGowan (2004), Nonlinear acoustoelastic constants of dry and saturated rocks, *J. Geophys. Res.*, *109*, B10204, doi:10.1029/2004JB003262.
Zarembo, L., and V. Krasil'nikov (1971), Nonlinear phenomena in the propagation of elastic waves in solids, *Sov. Phys. Usp.*, *13*(6), 778–797.